Analysis of Starved EHL Line Contacts for Lubricants with Linear Pressure Viscosity Dependence

Anuradha Parinam[1], Ram Karan [2]
[1,2] Department of Mechanical Engineering, University Institute of Engineering and Technology, Kurukshetra University, Kurukshetra, INDIA

Corresponding Author Email: panuradhasachdeva@gmail.com

Abstract

Most of the available works in elastohydrodynamic lubrication (EHL) have been carried out considering exponential pressure-viscosity relationship. However, recently, some lubricants such as 2, 3-dimethylpentane, pure hydrocarbon, water/glycol solutions etc. are reported to show linear piezo-viscous response. The investigations carried out using exponential pressure-viscosity relation for such lubricants yield to large errors as they highly overestimate the film thickness values. Also, a major aspect of practical EHL behavior i.e. starvation effect still remains largely unexplored. Starvation refers to the inadequate filling of the conjunction and has a considerable effect on EHL characteristics such as film thickness and coefficient of friction. Therefore, a numerical analysis is carried out for lubricants exhibiting linear piezo-viscosity to analyze the influence of starvation in EHL line contacts. Starvation effect is modeled by shifting the inlet meniscus towards the contact zone. The Reynolds equation is discretized using finite differences and solved along with the load balance equation using Newton-Raphson technique.

Keywords: *EHL, Linear piezo-viscosity, Starvation, Line contact.*

1. Introduction

EHL is a form of hydrodynamic lubrication in which elastic deformation of the surfaces and pressure dependence of viscosity play a fundamental role in the generation of load carrying film, which is thick enough to separate the surfaces completely. The accurate prediction of lubricant film thickness and friction coefficient in EHL contacts involved in mechanical components such as gears, cams, rolling element bearings etc. has long been the focus of attention. Conventionally, EHL studies employed piezo-viscous relationships involving an exponential function of lubricant pressure. Dowson and Higginson [1] and Hamrock and Dowson [2] presented film thickness equations using exponential piezo-viscous response and Newtonian fluid model for EHL line and point contacts, respectively. However, recently, Kumar et al. [3] presented examples of some practical situations involving high operating temperatures, low viscosity lubricants and water/glycol solutions where the lubricant's piezo-viscous response is more closely described by a linear relationship. Low molecular weight liquids like a pure hydrocarbon, 2, 3-dimethylepentane [4], octane and toluene [5] exhibit a linear piezo-viscous response. In addition, concentrated contact lubrication using the process liquid of low molecular

weight exhibits a linear pressure viscosity relationship and also, same trend is observed for ordinary lubricants at very high temperatures [3]. Further, it was reported that the viscosity pressure relationship of an aircraft engine lubricants (eg. L7808 and L23699) is linear. In fact, Barus's coefficient (α_B) decreases linearly as temperature increases for water/glycol solution. However, water/glycol solution forms a thinner film than conventional lubricants under the same operating conditions [6]. Furthermore, a substantial difference between the piezo-viscosities (and hence, EHL behaviors) represented by a simple exponential and a linear relationship was observed [7]. The use of conventional film thickness formulas for such lubricants may lead to large errors in the estimation of film thickness values. Therefore, using the linear piezo-viscous relationship of Barus [8-9], Kumar et al. offered central film thickness formulas which were validated experimentally. Anuradha and Kumar [7] extended their work by developing central and minimum film thickness formulas for EHL line contacts using linear piezo-viscosity.

Most of the above works were accomplished by considering fully flooded conditions. However, sometimes contact zone suffers from shortage of lubricant supply which leads to thinning of lubricant film. This is known as "starvation". Moreover, due to inadequate filling of the conjunction, the EHL film generated is much thinner as compared to the corresponding fully-flooded film and therefore, traction coefficient is also very high. Starvation effect is found to be higher at high speeds, using high viscosity lubricants and limited lubricant supply [10]. The starved steady state EHL circular contact problem was studied by Chevalier, Lubrecht and Cann [10, 11] for grease lubricated contacts. The transient effect in EHL circular contacts was investigated by Dumont et al. [12] by introducing the surface feature effects such as micro-pitted surface. Venner et al. [13] performed the numerical simulations to study the deformation of transverse and isotropic harmonic waviness in EHL circular contacts under pure rolling in relation to lubricant supply to the contact. Kumar and Khonsari [14] studied the effect of starvation on traction and film thickness in Thermo-EHL line contacts with shear-thinning lubricants. Therefore, the present work focuses on the effect of starvation on film thickness and traction coefficient using lubricant with linear piezo-viscosity with Newtonian fluid model.

2. EHL Model

Reynolds Equation

The Reynolds equation which governs the generation of pressure in the EHL line contacts with compressible fluid in dimensionless form is:

$$\frac{\partial}{\partial X}\left(\frac{\bar{\rho}H^3}{\bar{\mu}}\frac{\partial P}{\partial X}\right) = K\frac{\partial}{\partial X}\left(\bar{\rho}H\right) \qquad \text{---- (1)}$$

where, $K = \frac{3}{4}\left(\frac{\pi}{W}\right)^2 \cdot U$

Film Thickness Equation

The film thickness equation in dimensionless form is:

$$H(X) = H_o + \frac{X^2}{2} + \frac{1}{\pi}\sum_{j=1}^{N} D_{ij} P_j \qquad \text{---- (2)}$$

where D_{ij} are the influence coefficients for a uniform mesh size ΔX :

$$D_{ij} = -\left(i - j + \frac{1}{2}\right)\Delta X\left[\ln\left(\left|i - j + \frac{1}{2}\right|\Delta X\right) - 1\right] + \left(i - j - \frac{1}{2}\right)\Delta X\left[\ln\left(\left|i - j - \frac{1}{2}\right|\Delta X\right) - 1\right] \qquad \text{---- (3)}$$

Boundary Conditions

The boundary conditions applicable are:

$$P = 0 \text{ at } X = X_{in} \qquad \text{---- (4)}$$

$$P = \frac{\partial P}{\partial X} = 0 \text{ at } X = X_o \qquad \text{---- (5)}$$

Density-Pressure Relationship

The following Tait's equation of state is used to describe density-pressure relationship:

$$\frac{\rho_o}{\rho} = \frac{V}{V_o} = 1 - \frac{1}{1 + K_o'}\ln\left[1 + \frac{p}{K_o}\left(1 + K_o'\right)\right] \qquad \text{---- (6)}$$

The constants K_o and K_o' for the present analysis are taken as $K_0^{'} = 10$ and $K_0 = 1.0\,\text{GPa}$ (same as used in Ref [7]).

Viscosity-Pressure Relationship

The present analysis uses linear form of piezo-viscous relation as given by Barus:

$$\mu = \mu_0\left(1 + \alpha_B p\right) \qquad \text{---- (7)}$$

where, α_B=linear pressure viscosity coefficient.

Load Equilibrium Equation

The load equilibrium equation in dimensionless form is:

$$\int_{X_{in}}^{X_o} P dX = \frac{\pi}{2} \qquad \text{---- (8)}$$

Percentage of Starvation

Percentage of starvation is the ratio of difference between film thickness in fully flooded condition and starved condition to the film thickness in fully flooded condition. Percentage of starvation is given as:

$$\phi = \frac{Film\ Thickness_{Fully\ Flooded} - Film\ Thickness_{Starved}}{Film\ Thickness_{Fully\ Flooded}} \quad \text{---- (9)}$$

Coefficient of Friction

Coefficient of friction is the ratio of shear force of lubricant over whole surface to the applied normal load. This is expressed in non-dimensional form as:

$$COF = \sqrt{\frac{8}{\pi W}\int_{X_{in}}^{X_o} \bar{\tau}(Y=0)dX} \quad \text{---- (10)}$$

where $\bar{\tau}$ is the non-dimensional shear stress.

3. Solution Procedure

The solution procedure consists of following steps as given below.

1. The solution begins by assuming an initial guess for the pressure distribution $[P_i]$, offset film thickness H_o and outlet boundary coordinate $[X_o]$.
2. The film profile $[H_i]$ is calculated using the pressure distribution $[P_i]$ in the film thickness Eq. (2).
3. The fluid properties ($\bar{\rho}$ and $\bar{\mu}$) are computed using Eqs. (6) and (7).
4. The Reynolds Equation (1) is discretized using a mixed second order central and first order backward differencing scheme to obtain the equations $f_i = 0$ (i=2 to N) as follows:

$$f_i = \varepsilon_{i+1/2}\frac{P_{i+1}-P_i}{\Delta X^2} - \varepsilon_{i-1/2}\frac{P_i - P_{i-1}}{\Delta X^2} - K\frac{\left[(\bar{\rho}H)_i - (\bar{\rho}H)_{i-1}\right]}{\Delta X} \quad \text{---- (11)}$$

where $\varepsilon_i = \left(\frac{\bar{\rho}H^3}{\bar{\mu}}\right)_i$

5. The load equilibrium Equation (8) is written in the following discrete form using Simpson's coefficients:

$$\Delta W = \sum_{j=2}^{N} C_j P_j - \frac{\pi}{2} = 0 \quad \text{---- (12)}$$

$$\text{where } C_j = \begin{cases} \Delta X/3 & j = N \\ 4\Delta X/3 & j = 2,4,6..... \\ 2\Delta X/3 & j = 3,5,7..... \end{cases} \quad \text{---- (13)}$$

6. The simultaneous system of N equations represented by discretized Reynolds Equation (11) and load equilibrium Equation (12) are solved using the Newton-Raphson technique similar to that illustrated by Kumar and Khonsari [15]. The N system unknowns are P_2, P_3, P_4,……, P_N and H_0. The matrix equation of this system is

$$\begin{bmatrix} \frac{\partial f_2}{\partial P_2} & \frac{\partial f_2}{\partial P_3} & \cdots & \frac{\partial f_2}{\partial P_N} & \frac{\partial f_2}{\partial H_0} \\ \frac{\partial f_3}{\partial P_2} & \frac{\partial f_3}{\partial P_3} & \cdots & \frac{\partial f_3}{\partial P_N} & \frac{\partial f_3}{\partial H_0} \\ \cdots & \cdots & \cdots & \cdots & \cdots \\ \cdots & \cdots & \cdots & \cdots & \cdots \\ \frac{\partial f_N}{\partial P_2} & \frac{\partial f_N}{\partial P_3} & \cdots & \frac{\partial f_N}{\partial P_N} & \frac{\partial f_N}{\partial H_0} \\ C_2 & C_3 & \cdots & C_N & 0 \end{bmatrix} \begin{bmatrix} \Delta P_2 \\ \Delta P_3 \\ \cdots \\ \cdots \\ \Delta P_N \\ \Delta H_0 \end{bmatrix} = - \begin{bmatrix} f_2 \\ f_3 \\ \cdots \\ \cdots \\ f_N \\ \Delta W \end{bmatrix} \quad \text{---- (14)}$$

7. The pressure distribution $[P_i]$ and offset film thickness are updated using the correction calculated above.

8. The steps 2-7 are repeated until the following convergence criteria are satisfied:

$$\frac{\left| \left[\sum_{i=1}^{N} P_i \right]_n - \left[\sum_{i=1}^{N} P_i \right]_{n-1} \right|}{\left| \left[\sum_{i=1}^{N} P_i \right]_{n-1} \right|} \le 10^{-5}, \quad \left| \frac{[H_o]_n - [H_o]_{n-1}}{[H_o]_{n-1}} \right| \le 10^{-4}$$

4. Results and Discussion

When inlet conjunction does not fill adequately with lubricant then there is shortage of supply of lubricant in contact area which leads to film thinning and even breakdown takes place. This is called starvation effect. In the present analysis, the starvation effect is investigated by shifting the position of inlet meniscus towards contact zone. The effect of starvation is observed at different value of loads, velocities, pressure-viscosity coefficients and equivalent radii.

Fully-flooded condition is considered to be at the position of inlet meniscus where negligible change in film thickness is observed. In Table 1, central film thickness (nm) at three different loads is shown with change in inlet meniscus position from X_{in}=-7 to X_{in}=-2. Percentage

of starvation is calculated at each position of inlet by assuming next value a fully-flooded condition. For example, percentage of starvation at X_{in} =-6 is calculated by assuming X_{in} =-7 as fully-flooded position. It can be seen that the percentage of starvation decreases as inlet is taken away from the contact zone. It is observed from Table 1 that after X_{in} =-4, there is a negligible change in percentage of starvation i.e. below one percent for all the three loads considered. Hence, X_{in} =-5 is considered as a fully flooded condition beyond which there is negligible change in percentage of starvation. Similarly, fully-flooded condition is checked at different speeds as shown in Table 2.

Table 1 Percentage of starvation at different loads

X_{in}	W=3x10^{-5}		W=1x10^{-4}		W=5.2x10^{-4}	
-	h_c	φ	h_c	φ	h_c	φ
-7	130.58	-	103.25	-	76.00	-
-6	130.22	0.3	102.80	0.4	75.79	0.3
-5	129.61	0.5	102.29	0.5	75.44	0.5
-4	128.99	0.5	101.78	0.5	74.95	0.7
-3	127.62	1	101.17	0.6	74.31	0.9
-2	121.82	4	99.85	1	73.46	1

Table 2 Percentage of starvation at different rolling speeds

X_{in}	U=10^{-12}		U=10^{-11}		U=10^{-10}	
-	h_c	φ	h_c	φ	h_c	φ
-7	23.02	-	103.25	-	478.79	-
-6	22.88	0.6	102.81	0.4	477.42	0.3
-5	22.72	0.7	102.29	0.5	475.18	0.5
-4	22.54	0.8	101.78	0.5	472.57	0.6
-3	22.34	0.9	101.17	0.6	466.49	1
-2	22.10	1	99.85	1	440.47	5

It is observed that X_{in} =-5 ensures the fully-flooded condition for different operating conditions. At this position, it is assumed that the effect of starvation is zero and inlet meniscus occupies enough lubricating oil. So, effect of starvation is studied by shifting the inlet meniscus position from X_{in}=-5 to X_{in} =-1.06 toward contact zone which starts from X=-1. Starved characteristics for pressure, film thickness, and coefficient of friction are investigated within this range.

4.1. Percentage of Starvation

Percentage of starvation is defined as the ratio of difference of film thickness in fully-flooded and starved condition to the fully-flooded conditions. In this section, starvation effect is investigated considering different loads, rolling speeds, pressure viscosity coefficients and equivalent radii. The range of input parameters used in the simulations is shown in Table 3.

Table 3 Range of Input Parameters

Parameter	Unit	Value
W	-	$3x10^{-5}$ - $5.2x10^{-4}$
U	-	10^{-12} – 10^{-10}
α_B	GPa^{-1}	10
R	m	0.01
E'	GPa	210
K_0	GPa	1
$K_0^{'}$	-	10

The variation of percentage of starvation is shown in fig. 1 for three different loads (W=$3x10^{-5}$, $1x10^{-4}$, $5.2x10^{-4}$). Percentage of starvation varies with the position of inlet meniscus (X_{in}). As apparent from fig 1, the percentage of starvation at X_{in}=-5 is zero for all the three loads which corresponds to the fully flooded condition. As position of inlet meniscus shifts towards contact zone (X_{in} =-1), an increase in percentage of starvation is observed. Further, at lower loads, an abrupt increase in percentage starvation is noticed however, with the increase in load, percentage of starvation decreases. For the highest load considered here (W=$5.2x10^{-4}$), starvation is noticed too late with a small value close to the contact zone. This is due to the fact that at high loads pressure distribution approaches the Hertzian pressure profile and therefore, the pressure builds up very near the contact zone which results in the reduction of the inlet zone.

Fig. 2 shows the variation of percentage of starvation with the position of inlet meniscus at different rolling speeds (U=10^{-12}, U=10^{-11}, U=10^{-10}). The starvation is zero at X_{in}=-5 due to the fully-flooded condition. Unlike the load, as inlet meniscus position is shifts towards contact zone a

rapid increase in starvation is found for higher speed (U=10^{-10}). This can be attributed to the fact that at higher speeds, excess amount of lubricant is dragged within conjunction which leads to thicker fluid film. When there is an inadequate lubricant supply, the contacts get starved to a high level which leads to the thinning of lubricant film and ultimately the breakdown of film can occur.

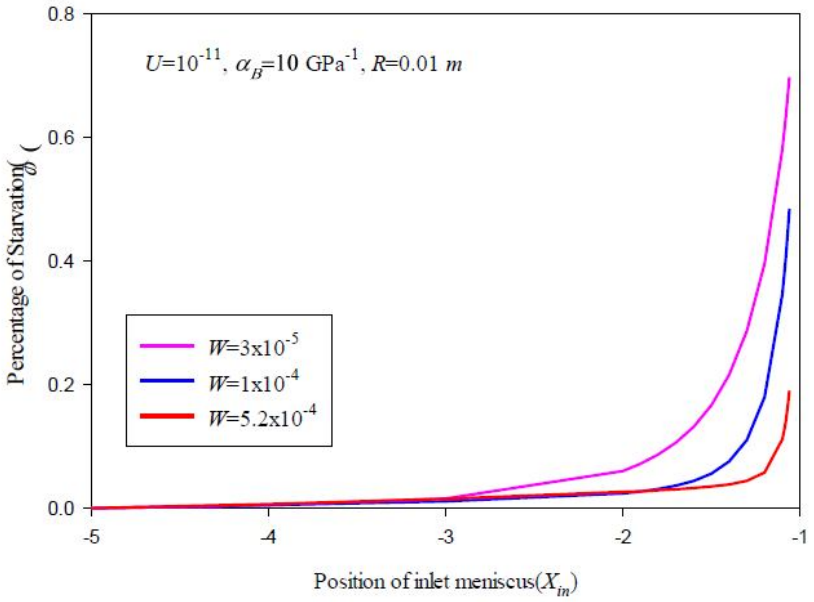

Fig. 1 Variation of percentage of starvation with the position of inlet meniscus for different loads at U=10^{-11}, α_B=10 GPa^{-1}, R=0.01 m.

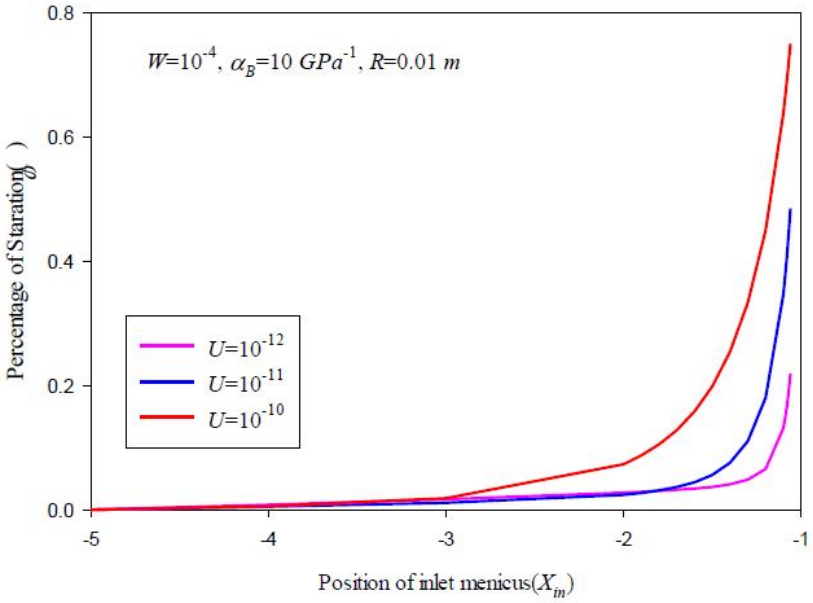

Fig. 2 Variation of percentage of starvation with the position of inlet meniscus for different rolling speeds at W=10^{-4}, α_B =10 GPa^{-1}, R=0.01 m.

4.2. Pressure Profile

Pressure distribution for two different inlet meniscus positions is shown in figures 3 and 4 for two different loads W=3x10^{-5} and W=5.2x10^{-4} respectively. One of inlet meniscus position is at fully-flooded condition (X_{in}=-5) and second (X_{in} =-1.06) is near the contact zone.

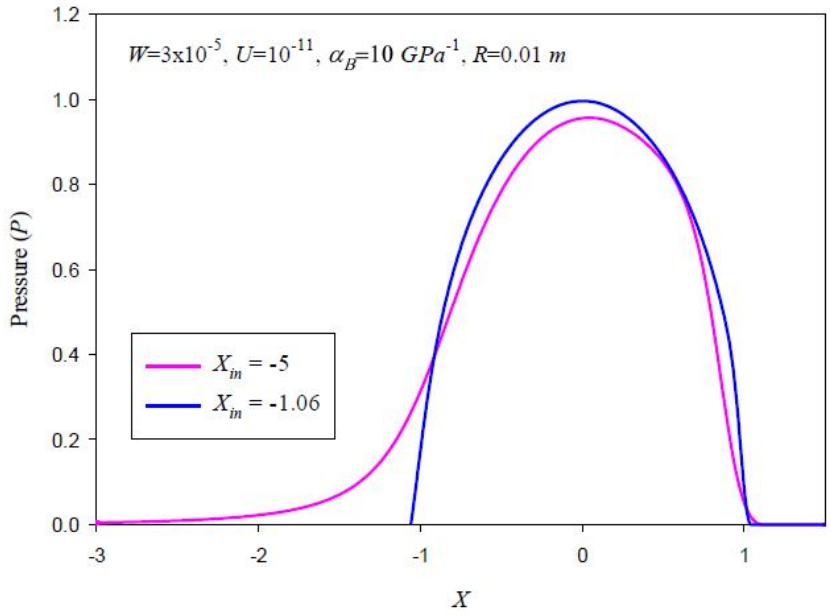

Fig. 3 Comparison of pressure profile at two different positions of inlet meniscus for U=10^{-12}, W=10^{-4}, α_B =10 GPa^{-1}, R=0.01 m.

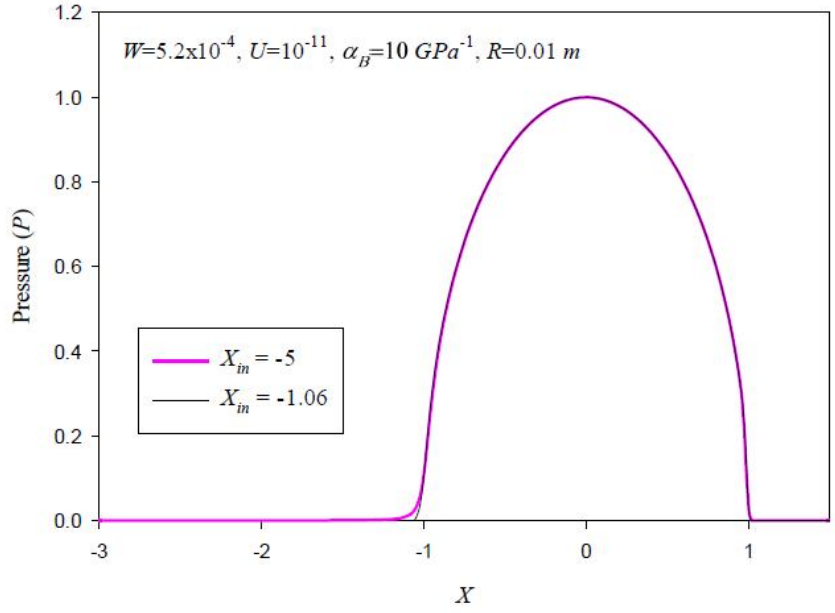

Fig. 4 Comparison of pressure profile at two different positions of inlet meniscus for U=10^{-10}, W=10^{-4}, α_B =10 GPa^{-1}, R=0.01 m.

It can be seen from fig. 3 that significant pressure builds up in the inlet zone for fully-flooded inlet meniscus position. However, only a marginal difference is observed in the central pressure values. On the other hand, the pressure profiles almost coincide at the higher value of load as seen in fig. 4.

Figures 5 and 6 show the effect of rolling speed on pressure distribution. It can be seen that at the lower speed (U=10^{-12}), the pressure profiles are almost coincident while at higher speed (U=10^{-10}), the pressure build up starts early for the fully flooded condition.

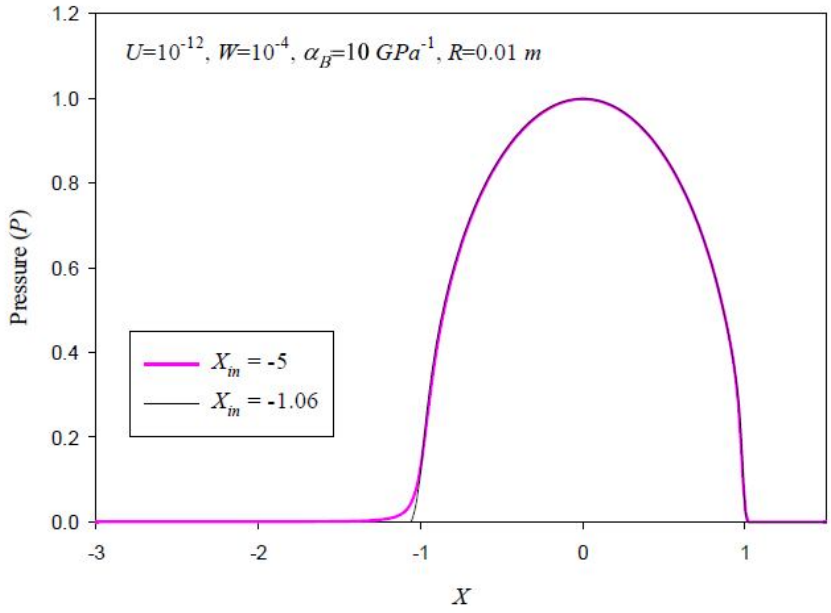

Fig. 5 Comparison of pressure profiles at two different positions of inlet meniscus for α_B =10 GPa^{-1}, W=10-4, U=10^{-11}, R=0.01 m.

4.3. Film Profile

Figures 7 and 8 show the film profiles at two different positions of inlet meniscus keeping other variables constant, at two different loads W=3x10^{-5} and W=5.2x10^{-4} respectively. It can be observed from both these figures that the film thickness obtained at X_{in} =-5 is greater than the film thickness at X_{in} =-1.06.

This is due to the starvation effect which is much more near the contact zone. However, it can be seen from fig. 10 that at higher value of load, the film thickness profile at two different position of inlet meniscus has a little difference. This shows that the effect of starvation is less pronounced at higher load at both inlet meniscus positions. This is due to the fact that the pressure distribution in contact zone approaches to Hertzian pressure and shrinkage of inlet zone takes place which minimize the effect of starvation.

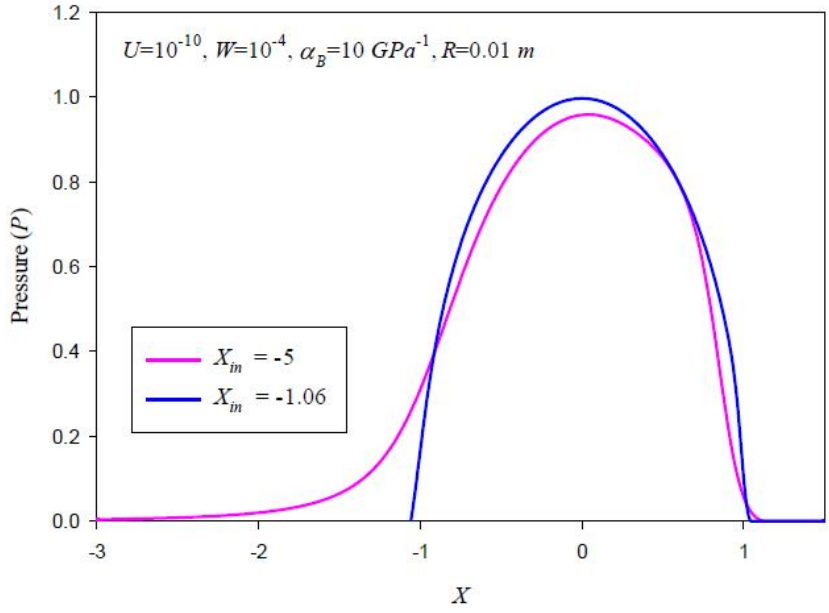

Fig. 6 Comparison of pressure profile at two different positions of inlet meniscus for α_B =10 GPa^{-1}, W=10^{-4}, U=10^{-11}, R=0.01 m.

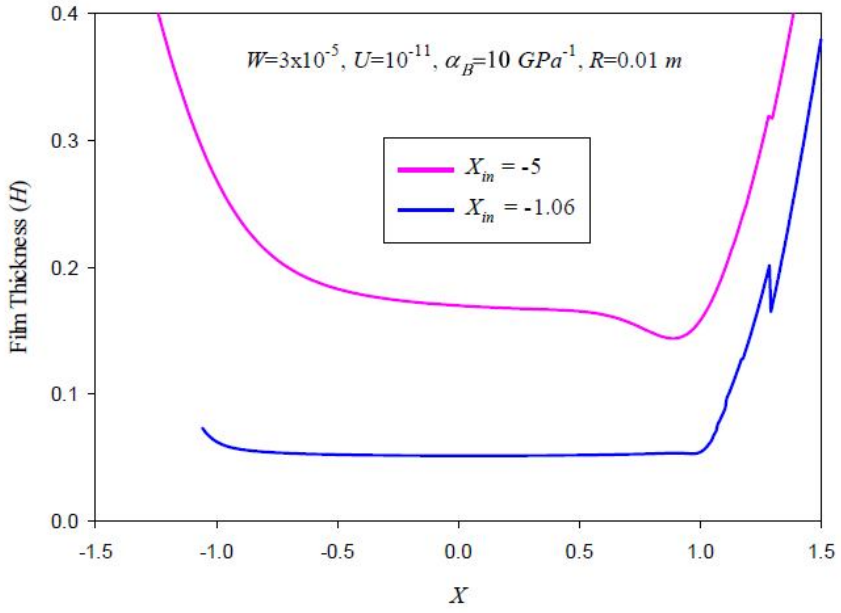

Fig. 7 Comparison of film profile at two different positions of inlet meniscus for W=3x10^{-5}, U=10^{-11}, α_B =10 GPa^{-1}, R=0.01 m.

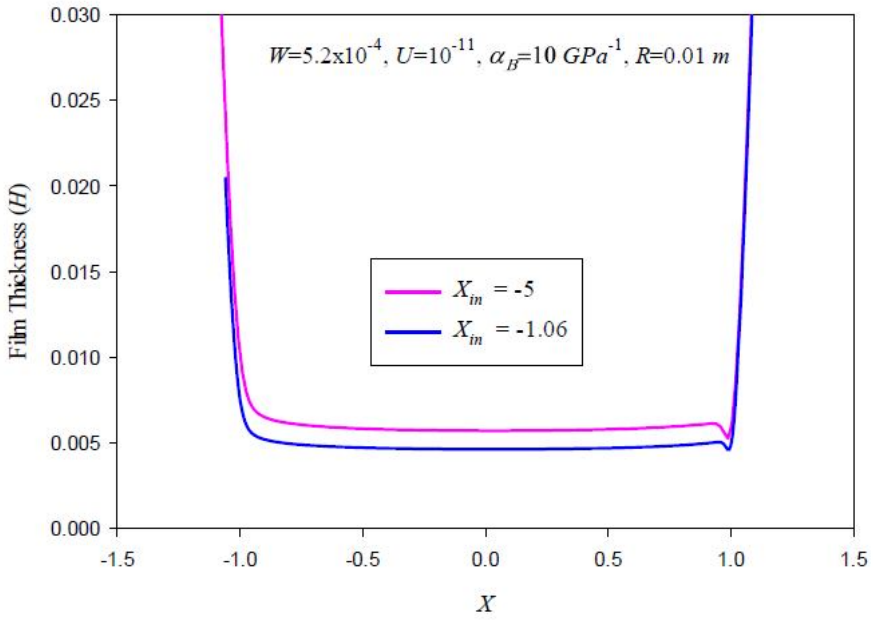

Fig. 8 Comparison of film profiles at two different positions of inlet meniscus for W=5.2x10^{-4}, U=10^{-11}, α_B =10 GPa^{-1}, R=0.01 m.

The effect of rolling speed on the film profile is shown in fig. 9 and 10 for two different positions of inlet meniscus at U=10^{-12} and U=10^{-10} respectively. It can be observed that unlike the load, the effect of starvation is more pronounced at higher rolling speed. Film thickness is much thinner at X_{in} =-1.06 in comparison with the film thickness at X_{in} =-5.

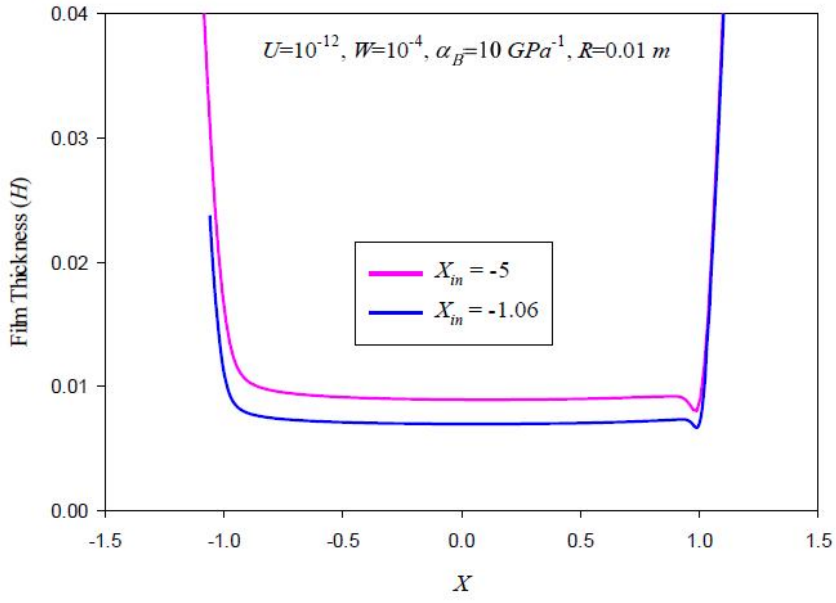

Fig. 9 Comparison of film profiles at two different positions of inlet meniscus for U=10^{-12}, W=10^{-4}, α_B=10 GPa^{-1}, R=0.01 m.

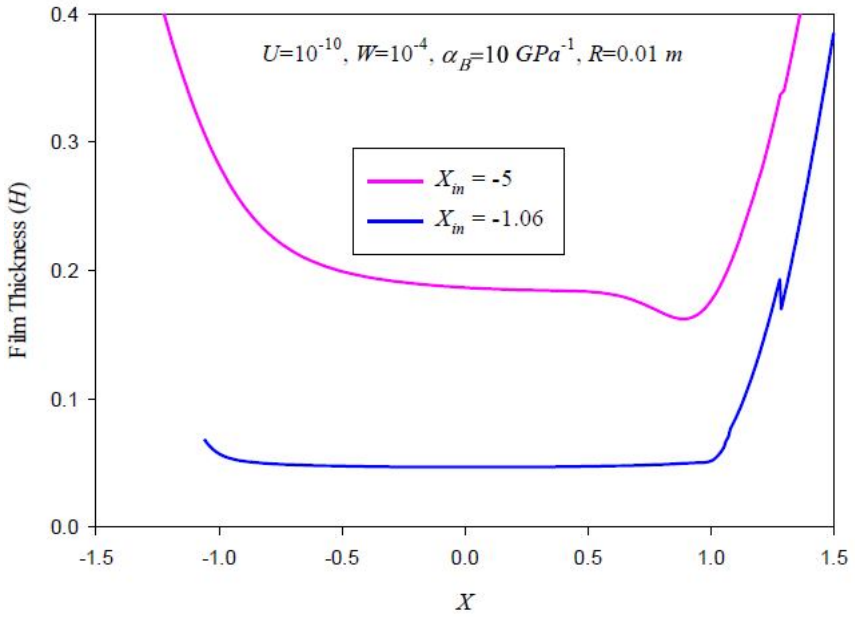

Fig. 10 Comparison of film profiles at two different positions of inlet meniscus for U=10^{-10}, W=10^{-4}, α_B=10 GPa^{-1}, R=0.01 m.

As the lubricating film needs to be thicker at such high speeds, excess lubricant needs to be supplied which lead to shortage of lubricant at inlet zone.

4.4. Coefficient of Friction

Fig. 11 shows the variation in $COF_{Starved}/COF_{Fully\text{-}Flooded}$ with the percentage of starvation (φ) at three different loads, W=3x10^{-5}, W=1x10^{-4}, W=5.2x10^{-4}. Coefficient of friction rises with rise in percentage of starvation. It can be seen from the figure that there is a steep increase in the friction value at lower load (W=3x10^{-5}) in comparison with other two loads. This is because high starvation at lower load, the film gets thinner and offers much friction to the moving surfaces which increase the coefficient of friction.

Fig. 12 compares the ratio of coefficient of friction with the percentage of starvation at three different speeds, U=10^{-12}, U=10^{-11}, U=10^{-10}. There is continuous rise in coefficient of friction with the increase in percentage of starvation at all speeds. However, a huge rise in coefficient of friction is noticed for higher speed, U=10^{-10}. This is attributed to high starvation effect at high rolling speed as discussed in previous sections. Due to high starvation, contact zone suffers from shortage of lubricant supply and film gets thinner to large extent and rubbing of surface takes place which increase the coefficient of friction.

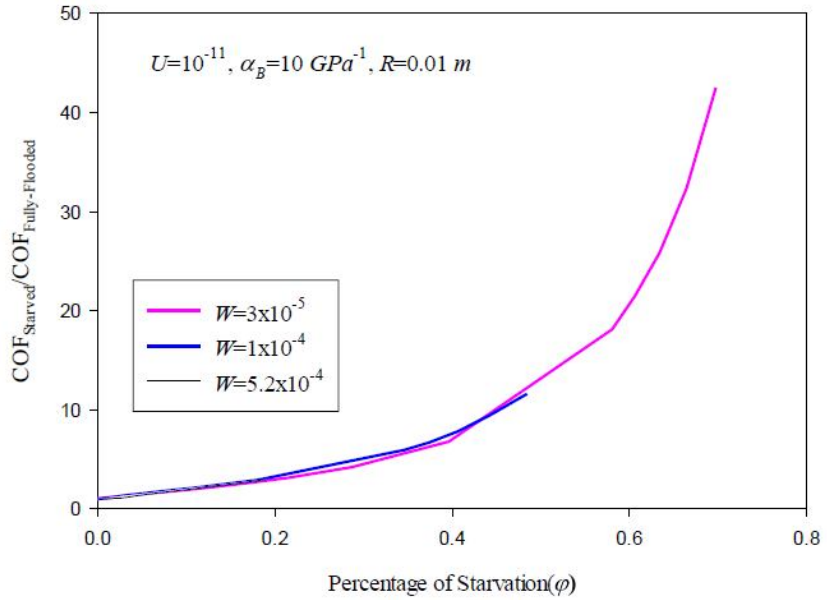

Fig.11 Comparison of factor by which coefficient of friction increases with the percentage of starvation for different loads at U=10^{-11}, α_B =10 GPa^{-1}, R=0.01 m.

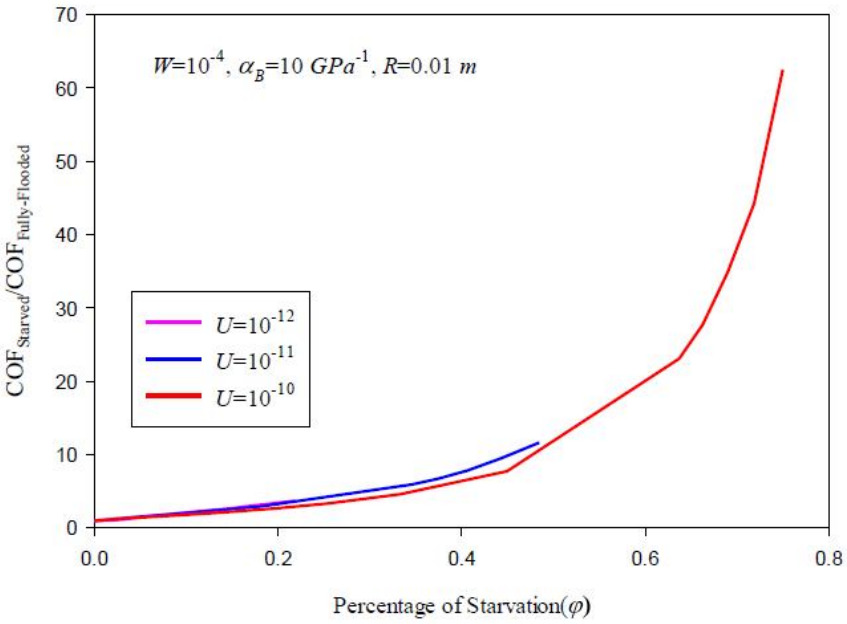

Fig. 12 Comparison of factor by which coefficient of friction increases with the percentage of starvation for different speeds at W=10^{-4}, α_B =10 GPa^{-1}, R=0.01 m.

5. Conclusions

A comprehensive EHL analysis is carried out to study the starvation effect on pressure distribution, film profile and coefficient of friction by changing the position of inlet meniscus for a lubricant exhibiting linear piezo-viscosity. It is found that starvation has a great influence on the film thickness and coefficient of friction. Starvation is largely influenced by rolling speed and viscosity of lubricant. Following are some of the salient conclusions:

1. Starvation is negligible in fully-flooded conditions and increases continuously while shifting inlet meniscus toward contact zone. It has been observed that it has maximum value near contact zone.

2. Starvation increases rapidly with increase in rolling speed. However, starvation effect decreases with increase in load. It is due to the fact that the pressure distribution in contact zone approaches to Hertzian pressure and shrinkage of inlet zone takes place which minimize the effect of starvation.

3. It has been observed that both pressure distribution and film profile are not affected by starvation at high load and low velocity. However, pressure profile has a significant difference for fully-flooded conditions and starved conditions at low load and high velocity, which is attributed to lower starvation at high load and low speed.

4. Coefficient of friction increases rapidly with increase in rolling speed. This is due to the fact that starvation is higher at high rolling speeds. Due to high value of starvation the contact zone suffers from lack of lubricant supply and thus, film gets thinner to a large extent and rubbing of surfaces takes place which lead to high value of coefficient of friction.

Nomenclature

Dimensional Parameters

b : half width of Hertzian contact zone, $b = 4R\sqrt{W/2\pi}$, (m**)**

E' : effective elastic modulus of rollers, $E' = 2/\left[\left(1-\nu_1^2\right)/E_1 + \left(1-\nu_2^2\right)/E_2\right]$ (Pa).

h : film thickness (m)

h_c : central film thickness (m)

$h_{\min}$: minimum film thickness (m)

p : pressure (Pa)

p_H : maximum Hertzian pressure, $p_H = E'b/4R$, (Pa)

R : equivalent radius of contact (m).

u_o : average rolling speed, $u_o = (u_1 + u_2)/2$, (m/s)

u_1, u_2 : velocities of lower and upper surfaces, respectively (m/s)

w : applied load per unit length (N/m)

Greek Symbols

α : Bridgman (exponential) piezo-viscous coefficient (Pa^{-1})

α_B : Barus (linear) piezo-viscous coefficient (Pa^{-1})

ρ_o : inlet density of the lubricant (kg/m^3)

ρ : lubricant density at the local pressure and temperature (kg/m^3)

μ_o : low-shear viscosity at p=0 (Pa.s)

μ : limiting low-shear viscosity at local pressure (Pa.s)

Dimensionless Parameters

G : classical dimensionless load parameter, $G = \alpha\ E'$

G_B : dimensionless load parameter, $G = \alpha_B E'$

H : dimensionless film thickness, $H = hR/b^2$

H_o : dimensionless offset film thickness

K_0 : isothermal bulk modulus at p = 0 (Pa)

K_0' : pressure rate of change of isothermal bulk modulus at p = 0

P : dimensionless pressure, $P = p/p_h$

U : dimensionless speed parameter, $U = \dfrac{\mu_o u_o}{E'R}$

W : dimensionless load parameter, $W = \dfrac{w}{E'R}$

X : coordinate in the direction of surface velocity (m), $X = x/b$

Greek Symbols

$\overline{\rho}$: dimensionless fluid density, $\overline{\rho} = \rho / \rho_o$

$\overline{\mu}$: dimensionless viscosity, $\overline{\mu} = \mu / \mu_o$

References

[1] Dowson, D. and Higginson G.R., "Elastohydrodynamic Lubrication", Oxford: Pergamon Press, 1966.

[2] Hamrock B.J. and Dowson D., "Ball Bearing Lubrication–The Elastohydrodynamics of Elliptical Contacts", New York: John Wiley & Sons, 1981.

[3] Kumar, P., Bair, S., Krupka, I. and Hartl, M., "Newtonian Quantitative Elastohydrodynamic Film Thickness with Linear Piezo-Viscosity," Tribology International, 43, 2010, pp. 2159-2165.

[4] Pensado, A., Comunas M.J.P., Lugo L., and Fernandez J., "Experimental dynamic viscosities of 2, 3-Dimethylpentane up to 60 MPa and from (303.15 to 353.15) K using a rolling-ball viscometer". Journal of Chemical Engineering Data, 50, 2005, pp. 849-855.

[5] Harris, K. R., Malhotra, R. and Woolf, L. A., "Temprature and Density Dependence of the Viscosity of Octane and Toluene," Journal of Chemical Engineering Data, 42, 1997, pp. 1254-60.

[6] Spikes, H.A., "Wear and Fatigue Problems in Connection with Water Based Hydraulic Fluids," Journal of Synthetic Lubrication, 4(2), 1987, pp. 115-35.

[7] Anuradha, P. and Kumar, P., "EHL Line Contacts Central and Minimum Film Thickness Equations for Lubricants with Linear piezo-viscous Behavior" Tribology International, 44, 2011, pp. 1257-1260.

[8] Barus, C., "Notes on the Dependence of Viscosity on Pressure and Temprature," Proc American Arts Science, 27, 1891, pp.13-8.

[9] Barus, C., "Isothermal, Isopiestics and Isometrics Relative to Viscosity" Am Journal of Science, 266, 1893, pp. 87-96.

[10] Chevalier, F., Lubrechet, A.A., Cann, P.M.E., Colin, F., and Dalmaz, G., "Starvation Phenomena in EHL Point Contacts: Influence of Inlet Flow Distribution", Proceedings of 22nd Leeds-Lyon Symposium on Tribology, Elseviers Tribology Series, 31, 1995, pp. 213-223.

[11] Chevalier, F., Lubrechet, A.A., Cann, P.M.E., Colin, F., and Dalmaz, G., "Film Thickness in Starved in Starved EHL Point Contacts", ASME Journal of Tribolgy, 120, 1998, pp. 126-133.

[12] Dumont, M.L., Lugt, P.M., and Tripp, J.H., "Surface Feature Effects in Starved Circular EHL Contacts", ASME Journal of Tribolgy, 124(2), 2001, pp. 358-366.

[13] Venner, C.H., Berger, G., and Lugt, P.M., "Waviness Deformation in Starved EHL Circular Contacts", ASME Journal of Tribolgy, 126(2), 2004, pp. 248-257.

[14] Kumar, P. and Khonsari, M.M., "Effect of Starvation on Traction and Film Thickness in Thermo-EHL Line Contacts with Shear-Thinning Lubricants", Tribology Letters, 32, 2008, pp. 171-177.

[15] Kumar P. and Khonsari M.M., "Combined Effects of Shear Thinning and Viscous Heating on EHL Characteristics of Rolling/Sliding Line Contact", ASME Journal of Tribolgy, 130, 2008, pp. 041505-1-13.